Photonic bandgap fibers with resonant structures for tailoring the dispersion

Z. Várallyay[1], K. Saitoh[2], Á. Szabó[3], and R. Szipőcs[4]

[1]*Furukawa Electric Institute of Technology Ltd., Vasgolyó u. 2-4, H-1158 Budapest, Hungary*
[2]*Graduate School of Information Science and Technology, Hokkaido University, Sapporo 060-0814, Japan*
[3]*Budapest University of Technology and Economics, Magyar tudósok körútja 2., H-1117 Budapest, Hungary*
[4]*Research Institute for Solid State Physics and Optics, P.O. Box 49, H-1525 Budapest, Hungary*

z.varallyay@feti.hu

Abstract: Numerical simulations on different kinds of realistic photonic bandgap fibers exhibiting reversed dispersion slope for the propagating fundamental mode are reported. We show that reversed or flat dispersion functions in a wide wavelength range using hollow-core, air-silica photonic bandgap fibers and solid core Bragg fibers with step-index profile can be obtained by introducing resonant structures in the fiber cladding. We evaluate the dispersion and confinement loss profiles of these fibers from the Helmholtz eigenvalue equation and the calculated fiber properties are used to investigate the propagation of chirped femtosecond pulses through serially connected hollow core fiber compressors.

OCIS codes: (060.2280) Fiber design and fabrication; (060.5295) Photonic crystal fibers; (190.7110) Ultrafast nonlinear optics.

References and links

1. P. St. J. Russell, "Photonic-Crystal Fibers," J. Lightwave Technol. **24,** 4729–4749 (2006).
2. C. K. Nielsen, K. G. Jespersen, and S. R. Keiding, "A 158 fs 5.3 nJ fiber-laser system at 1μm using photonic bandgap fibers for dispersion control and pulse compression," Opt. Express **14,** 6063–6068 (2006).
3. A. Ruehl, O. Prochnow, M. Engelbrecht, D. Wandt, and D. Kracht, "Similariton fiber laser with a hollow-core photonic bandgap fiber for dispersion control," Opt. Lett. **32,** 1084–1086 (2007).
4. C. de Matos, J. Taylor, T. Hansen, K. Hansen, and J. Broeng, "All-fiber chirped pulse amplification using highly-dispersive air-core photonic bandgap fiber," Opt. Express **11,** 2832–2837 (2003).
5. H. Lim, F. Ilday, and F. Wise, "Femtosecond ytterbium fiber laser with photonic crystal fiber for dispersion control," Opt. Express **10,** 1497–1502 (2002).
6. J. W. Nicholson, S. Ramachandran, and S. Ghalmi, "A passively-modelocked, Yb-doped, figure-eight, fiber laser utilizing anomalous-dispersion higher-order-mode fiber," Opt. Express **15,** 6623–6628 (2007).
7. J. Jasapara, Tsing Hua Her, R. Bise, R. Windeler, and D. J. DiGiovanni, "Group-velocity dispersion measurements in a photonic bandgap fiber," J. Opt. Soc. Am. B **20,** 1611–1615 (2003).
8. J. Lægsgaard, N. A. Mortensen, J. Riishede, and A. Bjarklev, "Material effects in air-guiding photonic bandgap fibers," J. Opt. Soc. Am. B **20,** 2046–2051 (2003).
9. D. Ouzounov, C. Hensley, A. Gaeta, N. Venkateraman, M. Gallagher, and K. Koch, "Soliton pulse compression in photonic band-gap fibers," Opt. Express **13,** 6153–6159 (2005).
10. Z. Várallyay, K. Saitoh, J. Fekete, K. Kakihara, M. Koshiba, and R. Szipőcs, "Reversed dispersion slope photonic bandgap fibers for broadband dispersion control in femtosecond fiber lasers," Opt. Express **16,** 15603–15616 (2008).
11. J. Jasapara, R. Bise, T. Her, and J. W. Nicholson, "Effect of Mode Cut-Off on Dispersion in Photonic Bandgap Fibers," in Optical Fiber Communication Conference, Technical Digest (Optical Society of America, 2003), paper **ThI3**.

#111521 - $15.00 USD Received 19 May 2009; revised 20 Jun 2009; accepted 22 Jun 2009; published 29 Jun 2009

12. T. Engeness, M. Ibanescu, S. Johnson, O. Weisberg, M. Skorobogatiy, S. Jacobs, and Y. Fink, "Dispersion tailoring and compensation by modal interactions in OmniGuide fibers," Opt. Express **11,** 1175–1196 (2003).
13. Q. Fang, Z. Wang, L. Jin, J. Liu, Y. Yue, Y. Liu, G. Kai, S. Yuan, and X. Dong, "Dispersion design of all-solid photonic bandgap fiber," J. Opt. Soc. Am. B **24,** 2899–2905 (2007).
14. P. J. Roberts, "Control of dispersion in hollow core photonic crystal fibers," Conference on Lasers and Electro-Optics 2007 CLEO proceedings 2007, p. 1630, presentation **CWF2**.
15. J. Lægsgaard, P. J. Roberts and M. Bache, "Tailoring the Dispersion Properties of Photonic Crystal Fibers," Optical and Quantum Electronics **39,** 995–1008 (2007).
16. J. Kuhl and J. Heppner, "Compression of femtosecond optical pulses with dielectric multilayer interferometers," IEEE Trans. Quant. Electron. **QE-22,** 182–185 (1986).
17. H. A. Macleod, Thin-film optical filters third edition, (J W Arrowsmith Ltd, Bristol, GB 2001).
18. J. Fekete, Z. Várallyay and R. Szipőcs, "Design of high-bandwidth one- and two-dimensional photonic bandgap dielectric structures at grazing incidence of light," Appl. Opt. **47,** 5330–5336 (2008).
19. R. Szipőcs, A. Kőházi-Kis, S. Lakó, P. Apai, A. P. Kovács, G. DeBell, L. Mott, A. W. Louderback, A. V. Tikhonravov, and M. K. Trubetskov, "Negative dispersion mirrors for dispersion control in femtosecond lasers: chirped dielectric mirrors and multi-cavity Gires-Tournois interferometers," Appl. Phys. B **70,** S51-S57 (2000).
20. K. Saitoh and M. Koshiba, "Leakage loss and group velocity dispersion in air-core photonic bandgap fibers," Opt. Express **11,** 3100–3109 (2003).
21. K. Saitoh, N.J. Florous, T. Murao, and M. Koshiba, "Realistic design of large-hollow-core photonic band-gap fibers with suppressed higher order modes and surface modes," J. Lightwave Technol. **25,** 2440–2447 (2007).
22. M. Sumetsky and S. Ramachandran, "Multiple mode conversion and beam shaping with superimposed long period gratings," Opt. Express **16,** 402-412 (2008).
23. J. C. Jasapara, M. J. Andrejco, A. D. Yablon, J. W. Nicholson, C. Headley, and D. DiGiovanni, "Picosecond pulse amplification in a core-pumped large-mode-area erbium fiber," Opt. Lett. **32,** 2429–2431 (2007).
24. P. J. Roberts, D. P. Williams, B. J. Mangan, H. Sabert, F. Couny, W. J. Wadsworth, T. A. Birks, J. C. Knight, and P. St. J. Russell, "Realizing low loss air core photonic crystal fibers by exploiting an antiresonant core surround," Opt. Express, **13,** 8277–8285 (2005).
25. T. Murao, K. Saitoh, and M. Koshiba, "Structural optimization of air-guiding photonic bandgap fibers for realizing ultimate low loss waveguides," J. Lightwave Technol., **26,** 1602–1612, (2008).
26. C. J. Hensley, D. G. Ouzounov, A. L. Gaeta, N. Venkataraman, M. T. Gallagher, and K. W. Koch, "Silica-glass contribution to the effective nonlinearity of hollow-core photonic band-gap fibers," Opt. Express **15,** 3507–3512 (2007).
27. L. Vincetti, M. Maini, F. Poli, A. Cucinotta, and S. Selleri, "Numerical analysis of hollow core photonic band gap fibers with modified honeycomb lattice," Opt. and Quantum Electron., **38,** 903–912 (2006).
28. J. Lægsgaard, N. A. Mortensen, and A. Bjarklev, "Mode areas and field-energy distribution in honeycomb photonic bandgap fibers," J. Opt. Soc. Am. B, **20,** 2037–2045 (2003).
29. G. P. Agrawal, *Nonlinear Fiber Optics*, fourth edition (Academic, San Diego, CA, 2007) Chapter 2.
30. Z. Várallyay, J. Fekete, Á. Bányász and R. Szipőcs, "Optimizing input and output chirps up to the third-order for sub-nanojoule, ultra-short pulse compression in small core area PCF," Appl. Phys. B **86,** 567–572 (2007).

1. Introduction

Photonic bandgap (PBG) fibers [1] are attractive candidates to achieve high quality pulse compression in fiber lasers [2, 3] or amplifiers [4] at the Ytterbium wavelengths or wavelength regions where systems exhibit normal cumulative dispersion. The compression with these fibers can be obtained by splicing the appropriate length into the cavity or after the output as it is already demonstrated by microstructured fibers [5] or higher order mode fibers [6]. Two properties of hollow-core PBG fibers offer this opportunity: (i) the dispersion is mostly anomalous around the center of the bandgap [7] and (ii) the propagating mode is confined in a hollow core which may result in low nonlinearity [8]. The first property can provide a spectral phase shift of an opposite sign on the pulse than experienced by the contributions from other system components which may reduce the temporal width of the pulse. The latter property allows us to avoid large nonlinear phase shifts at elevated intensities which effect would change the spectral shape and introduces an additional positive linear chirp on the pulse.

PBG fibers, however, have a significant third order dispersion contribution to the pulse evaluation which results in a residual higher order spectral phase on the pulse responsible for asymmetries. This phenomenon limits the maximum compression ratio of the pulses that can be

#111521 - $15.00 USD Received 19 May 2009; revised 20 Jun 2009; accepted 22 Jun 2009; published 29 Jun 2009

achieved by HC fibers [9]. An ideal fiber compressor, namely, should have anomalous dispersion which is usually given at PBG fibers and negative dispersion slope (DS) which can be realized by careful structural modifications [10].

The dispersion of PBG fibers that changes a resonant way was first observed in high index liquid field microstructured fibers [7, 11] which resembled to that of Fabry-Pérot resonances. Introducing geometrical defects in the perfectly periodic structure of a PBG cladding results in a modified group-delay dispersion and even negative dispersion slope was first shown in HC OmniGuide fibers [12]. Dispersion modification in all-glass PBG fibers was also initiated by the introduction of defect rods in the cladding region [13]. This modification shifted and changed the magnitude of the dispersion function. It was also shown that dispersion modification did work for HC PBG fibers by changing the first period of the fiber avoiding this way the anti-crossing events within the bandgap [14]. The resulted dispersion function was a nearly flat function over a wide wavelength range with very small positive dispersion slope. Negative dispersion slope for HC fibers was also predicted by resonant layers changing the hole size and the shape of the holes in the first and second periods of a HC fiber [15]. The used resonant layers in the cladding are very similar to those ones we are introducing in the case of HC fibers but digging into theory lower order resonances (using thinner layers not thicker ones than the original period) also can be found.

We aim to apply resonant structures resembling to that of Gires-Tournois interferometers (GTI) around the core in solid-core (SC) and HC fibers taking the analogy from one dimensional PBG structures. GTIs have an arrangement similar to Fabry-Pérot (FP) interferometers. Whereas FP cavity is enclosed by two high-reflecting mirrors, GTIs consist of both a high and a low reflector which results in a highly frequency dependent phase shift on the light field falling on the low-reflectivity surface [16].

In this paper we detail the theory of GTI in a PBG fiber and aim to design realistic PBG cladding structures yielding reversed or flat dispersion profiles around the Ytterbium wavelengths. In contrast of our previous study where we applied higher order modes to obtain the required dispersion profile [10] we show that proper structural changes may yield reversed dispersion slope (RDS) over a wide wavelength range (100-200 nm) for the propagating fundamental core mode too. We investigate the coupling efficiency of the distorted mode due to resonant coupling with the GTI, the propagation loss, the fiber nonlinearity and also femtosecond pulse propagation is modeled using the calculated fiber properties. These simulations show that the designed fiber can be an essential tool to reach the sub-100 fs region with high power ($>$ 1W) all-fiber devices.

2. Theory

Think of GTI as a thin film (TF) with 100% reflection at one side where the high reflectance is ensured by the fiber cladding in a photonic crystal fiber (PCF) and low reflection at the other side: core-TF interface as shown in Fig. 1. The amplitude reflection of this layer can be given by [17]

$$\rho = \frac{\eta_0 - A}{\eta_0 + A} \tag{1}$$

where η_0 is the admittance of the incident medium (core) and A is the admittance of the GT layer which can be determined by the evaluation of the electric and magnetic fields on the surfaces using the characteristic matrix yielding

$$A = \frac{\eta_2 \cos(\delta) + i\eta_1 \sin(\delta)}{\cos(\delta) + i(\eta_2/\eta_1)\sin(\delta)} \tag{2}$$

#111521 - $15.00 USD Received 19 May 2009; revised 20 Jun 2009; accepted 22 Jun 2009; published 29 Jun 2009

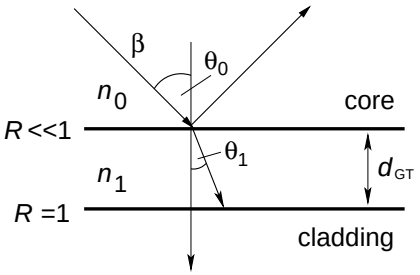

Fig. 1. Schematic illustration of a GT interferometer between core and cladding in a PBG fiber.

where η_2 is the admittance of the subsequent layers (the cladding) and δ is the phase factor of the positive going wave given by

$$\delta = \frac{\omega}{c} n_1 d_{GT} \cos(\theta_1) \tag{3}$$

where d_{GT} is the GT layer thickness, n_1 is the refractive index of TF, ω is the angular frequency of light, c is the speed of light in vacuum and θ_1 is the angle of refraction.

η_2 is zero in Eq. (2) since we assume that the reflectance is $100\% = (\eta_1 - \eta_2)/(\eta_1 + \eta_2)$ at this side of the TF which is a good approximation at the close center of the bandgap.

Writing back Eq. (2) into Eq. (1) with the above mentioned simplification ($\eta_2 = 0$) the amplitude refraction of a GT interferometer can be given by

$$\rho = \frac{\eta_0 - i\eta_1 \tan(\delta)}{\eta_0 + i\eta_1 \tan(\delta)} \tag{4}$$

The real and imaginary part of Eq. (4) is yielding the phase shift on the incident field as follows

$$\tan\phi = \frac{-2\eta_0\eta_1 \tan(\delta)}{\eta_0^2 + \eta_1^2 \tan^2(\delta)} \tag{5}$$

where the admittances at oblique incidence for the p-polarization component can be given by

$$\eta_0 = n_0 Y / \cos(\theta_0), \tag{6}$$

$$\eta_1 = n_1 Y / \cos(\theta_1) \tag{7}$$

where $Y = \sqrt{\varepsilon_0/\mu_0}$ is the admittance of the free space.

The group-delay (GD) ($d\phi/d\omega$), the group-delay dispersion (GDD) ($d^2\phi/d\omega^2$) and higher order dispersions can be easily derived from Eq. (5). The oblique incidence in our case is important due to the high propagation angle of light in fibers which prerequisite can be obtained from the corresponding eigenvalue of the investigated mode:

$$\theta_0 = \arcsin(n_{\text{eff}}/n_0) \tag{8}$$

where n_{eff} is the effective refractive index and n_0 is associated with the core index.

For the Bragg fiber investigated in the next section, the propagation angle obtained from the Helmholtz eigenvalue equation is approximately 87° for the fundamental mode. The refractive index of GTI is chosen to be $n_1 = 1.46$ and the core index is $n_0 = 1.45$ at around 1.03 μm. We plot the GD and GDD functions of the GTI based on Eq. (5) in Fig. 2 applying thicknesses that show the nonlinear phase shift and resonance behavior at around 1 μm. We found that

#111521 - $15.00 USD Received 19 May 2009; revised 20 Jun 2009; accepted 22 Jun 2009; published 29 Jun 2009

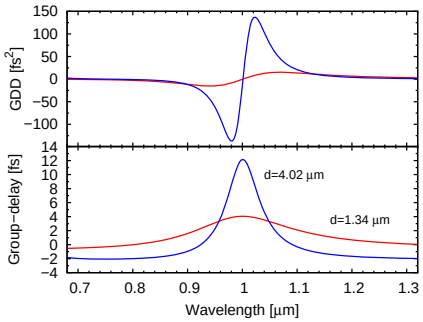

Fig. 2. First- and second-order resonances on GD and GDD curves of GT interferometer for oblique incidence with 4.02 and 1.34μm thicknesses, $n_0 = 1.45$, $n_1 = 1.46$ and $\theta_0 = 87^\circ$. Calculated from the derived Eq. (5).

the thickness of the GTI must be 1.34 μm (first-order resonance) or 4.02 μm (second-order resonance). The mediate thicknesses shift the position of the resonance peak. The reversed region of the GDD function is broader for the lower-order resonance and sharper for the higher-order one.

Photonic bandgap structures can be approximated well with one-dimensional dielectric structures [18] using *p*-polarization component of the light. Therefore, in the followings we demonstrate that GTI works for SC PBG fibers as well as for HC PBG fibers.

3. Solid core Bragg fibers

We realize the same GTI structure in a SC Bragg fiber than it is obtained from the analytical calculations above. The used structure is shown in Fig. 3. We found that if we use realistic high and low index materials for cladding with $n_L = 1.45$ and $n_H = 1.5$, than the optimum structure which shows a broad and regular bandgap with 10^{-6} dB/m confinement loss must have low index and high index layer thicknesses of 3.8 μm and 0.95 μm, respectively.

Two parameters can be adjusted in connection with the RDS; the refractive index and the thickness of the GT layer. We set the refractive index of the GT layer to 1.46, and thickness of it to $0.34d_L$ which results in a 180 nm RDS region from 960 nm to 1140 nm. Increasing the thickness of this resonant layer shifts the RDS region to longer wavelengths (Fig. 4(a)), while the increase in it's refractive index causes stronger resonances and steeper dispersion function due to the decreasing refraction on the first surface (core-GT interface). Figure 4(b) however, shows a high sensitivity on the changes of the GTI index. 0.1-0.2% index difference may cause almost 100 nm shift and some changes in the steepness of the DS. This shows that small deviations from the ideal conditions at manufacturing process may result an essentially different dispersion profile.

Nearly zero dispersion profile is also demonstrated in Fig. 4(b) for $n_{GT} = 1.458$, where the dispersion fluctuation is 12 ps/(nm·km) over a 280 nm wavelength range. Similarly, for $d_{GT} = 0.5d_L$ (Fig. 4(a)) the changes of the dispersion function is less than 4 ps/(nm·km) over an almost 200 nm wavelength range. The loss profiles show an acceptable loss (< 0.1 dB/m) when using these fibers for real applications. In Fig. 4(c) and Fig. 4(d), one can see that the wavelength range where dispersion tailoring is achieved falls on the increasing tail of the loss profile which indicates that the mode has continuously stronger resonant coupling with the GT layer, resulting in higher loss. In order to see the changes in the mode profile due to the resonance coupling we plotted the fundamental core mode at the short and long wavelength edge and in the middle of the reversed slope region in Fig. 5, corresponding to the GTI with $d_{GT} = 0.34d_L$ and $n_{GT} = 1.46$.

#111521 - $15.00 USD Received 19 May 2009; revised 20 Jun 2009; accepted 22 Jun 2009; published 29 Jun 2009

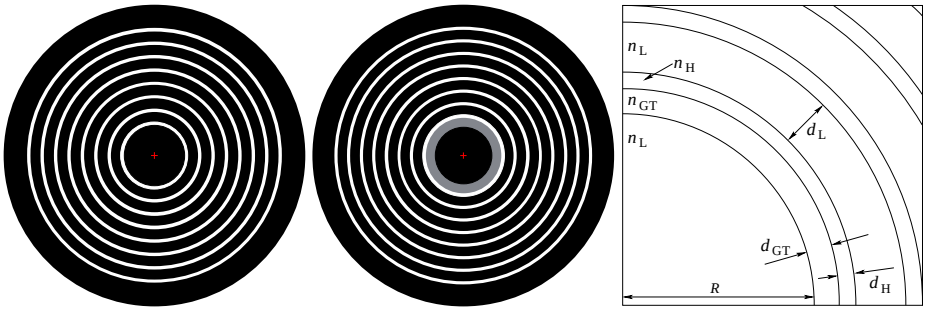

(a) (b) (c)

Fig. 3. (a) SC Bragg fiber with periodic annular layers, (b) SC Bragg fiber with a resonant first layer having a refractive index of n_{GT} and thickness of d_{GT} and (c) parameters of the fiber.

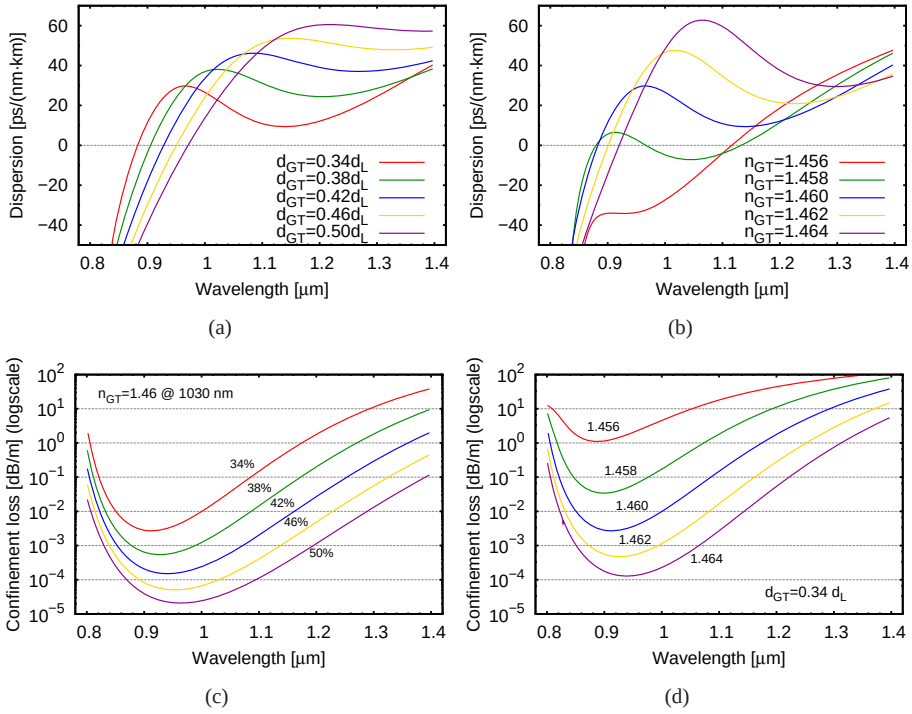

(a) (b) (c) (d)

Fig. 4. Dispersion and confinement loss profiles of different GTIs realized around the core in an SC Bragg PBG fiber. (a) dispersion functions with different thicknesses of GTI, (b) dispersion functions with GTI having different refractive indices, (c) confinement loss belonging to the case changing GTI thicknesses and (d) confinement loss with different GTI refractive indices.

#111521 - $15.00 USD Received 19 May 2009; revised 20 Jun 2009; accepted 22 Jun 2009; published 29 Jun 2009

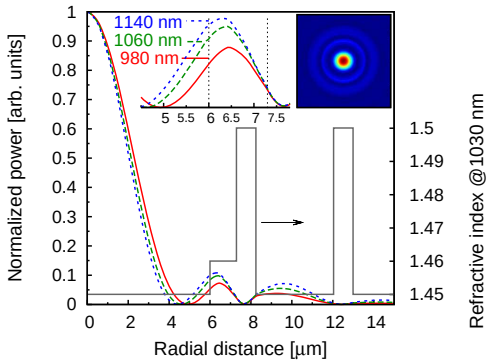

Fig. 5. Propagating fundamental mode profiles at 980 nm, 1060 nm and 1140 nm wavelengths. The embedded graph zooms to the close surrounding of GTI. Vertical black lines show the region where the refractive index $n_{\mathrm{GTI}} = 1.46$. Inset shows the 2D distribution of the propagating fundamental mode at 1060 nm. (Media 1)

The higher the light energy stored in the GTI is the larger group-delay of the propagating pulse can be expected as it is already demonstrated at one-dimensional PBG structures [19]. This is the reason that the presented resonant layer is able to reverse the dispersion function resulting in a wavelength dependent standing field in the GTI. The mode at the long wavelength edge of the reversed slope looks like more an LP_{02} than an LP_{01} mode due to resonant coupling of the fundamental mode with the GTI.

4. Air-silica hollow core PBG fibers

In the case of all-silica HC PBG fibers the resonant GT layer can be presented by a detuned first period [10] changing the thickness of the first air layer whose reflectance can be further reduced by decreasing the thickness of the core wall (first high index layer). The high reflector is the properly designed microstructured cladding where the high and low index layers satisfy the quarter wavelength condition (QW). The used model of HC PBG fiber with a honey-comb structured cladding and the necessary geometrical changes are shown in Fig. 6(a) and 6(b). In a 7-unit-cell HC-PBG fiber, core radius is determined by the hole-to-hole spacing Λ, the core wall thickness t and the introduced core expansion coefficient E

$$R_c = (E+1)(1.5\Lambda - t/2 \tag{9}$$

where the role of E is clearly to provide a larger core and a detuned first period with thin air-spacer layer (See the meanings of the parameters in Fig. 6(c)). The pitch was selected to $\Lambda = 2.85$ μm to obtain a bandgap centered around 1100-nm wavelength range and the hole size and pitch ratio to $d/\Lambda = 0.98$ which indicates a very high air-filling fraction in order to obtain large PBG in the cladding and lower the leakage losses [20]. The core wall thickness was $t = T(\Lambda - d)$ where T is a parameter usually smaller than unity. We can suppress the existence of surface modes which localize energy at the core wall by selecting $T < 0.5$ [21] at the RDS wavelengths.

In Fig. 7(a), and 7(b) we show the calculated dispersion profiles for the LP_{01}-like fundamental air-core mode for changing the T and E parameters, respectively, in a 7-cell-core PBG fiber. If $T = 0.3$ and $E = 0.18$, the obtained dispersion function is the one having a reversed dispersion slope around 1050 nm and it ranges from 1012 nm to 1106 nm. This 94 nm wide reversed slope region presented for the LP_{01}-like fundamental mode can be raised to 120 nm by setting

#111521 - $15.00 USD Received 19 May 2009; revised 20 Jun 2009; accepted 22 Jun 2009; published 29 Jun 2009

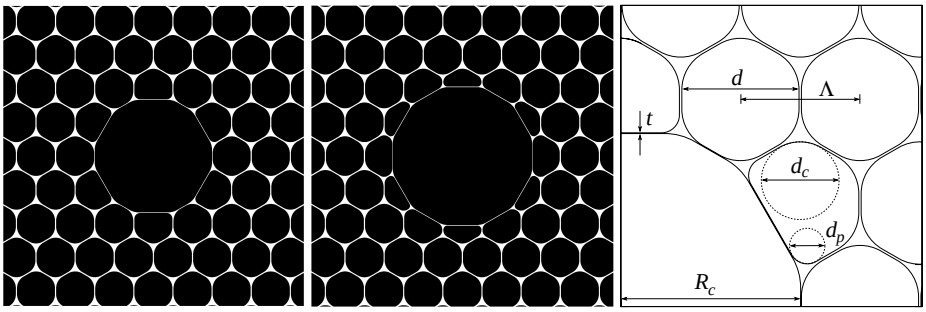

(a) (b) (c)

Fig. 6. Regular HC fiber structure (a), fiber structure with core expansion (b) and the model parameters (c).

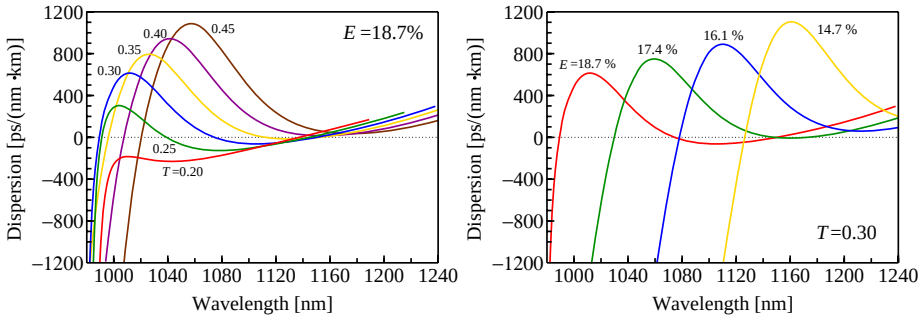

(a) (b)

Fig. 7. Dispersion functions of the designed HC PBG fiber with (a) different core wall thicknesses and (b) different core expansion coefficients.

$T = 0.45$ (see Fig. 7(a)). This increase in the core wall thickness introduces stronger resonance in the phase-delay of the light due to the increasing reflectance of the first facet light reaches during the propagation and consequently results in a steeper dispersion slope than those belonging to smaller T values. Decreasing the magnitude of the expansion coefficient (Fig. 7(b)) will shift the reversed slope region to longer wavelengths without changing the magnitude of the negative slope range. Namely, varying the thickness of the first low index layer will determine the position of the resonance property.

Because of the large index difference between the low and high index materials constituting the fiber cladding the resonant coupling with the GTI is also larger than in the case of SC Bragg fibers with smaller index differences, resulting in a much more distorted mode profile. Figure 8 shows the mode field distribution at 1000, 1050 and 1100 nm.

Figure 9 is intended to show the wavelength-dependence of the confinement loss for the fundamental air-core mode with and without GTI in hollow-core PBG fibers using 6 periods of air-holes in the cladding region. T is kept at 0.3 in both cases without core expansion as well as with $E = 0.187$. Due to the presence of resonances for $E = 0.187$, what we obtained is an elevated loss profile by almost three magnitudes, but still resulting in less than 0.01 dB/m which is acceptable for the purpose of dispersion management.

#111521 - $15.00 USD Received 19 May 2009; revised 20 Jun 2009; accepted 22 Jun 2009; published 29 Jun 2009

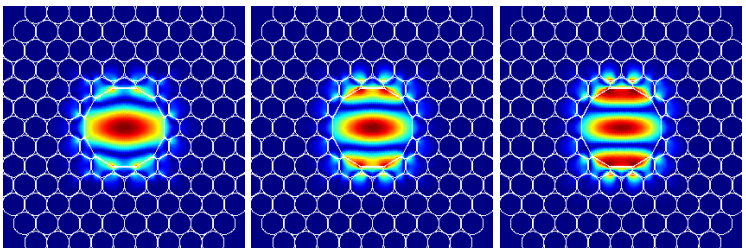

(a) (b) (c)

Fig. 8. Mode distribution for one particular polarization component of LP_{01} at (a) 1000 nm, (b) 1050 nm and (c) 1100 nm.

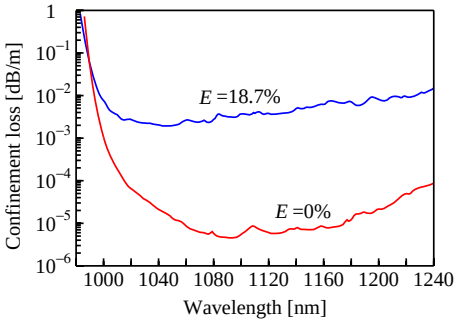

Fig. 9. Confinement losses of HC PBG fibers with $E = 0$ and $E = 0.187$ core expansion factors.

5. Coupling loss

Due to the mode distortions it is reasonable to investigate how large coupling loss can be expected when one splices the investigated fiber in Sec. 3 to an other Bragg or a step-index profiled fiber. We computed the overlap integral between the modes of the modified cladding structure and the modes of the fiber without GTI:

$$\mu(\lambda) = \int_0^{2\pi} \int_0^{\infty} \Psi^{(1)}(r,\phi,\lambda)\Psi^{(2)^*}(r,\phi,\lambda) r dr d\phi \tag{10}$$

where $\Psi^{(k)}$, $k = 1,2$ is the normalized electric field distribution in the kth fiber, and the symbol $*$ stands for complex conjugate. The results are summarized in Fig. 10(a) where we present the loss due to coupling the light from one fiber to another one between 900 and 1200 nm. First we tested the coupling between the unmodified Bragg fiber ($d_L = 3.8$ μm, $d_H = 0.95$ μm $n_L = 1.45$ and $n_H = 1.5$) and a step-index fiber having the same 6 μm core radius and an index difference between the core and cladding: $\Delta n = 0.0036$. The cladding refractive index follows the index of fused silica obtained from the Sellmeier equation at any wavelength. The overlap factor shows 81% coupling at 1040 nm which is equivalent with a 0.9dB loss (curve with full circles in Fig. 10(a)). By the introduction of the GT layer around the core in the Bragg fiber ($d_{GT} = 0.34 d_L$, $n_{GT} = 1.46$ at 1030 nm) and investigate the coupling to a Bragg fiber with the same cladding structure except the GTI, the overlap factor yields a value of 30% which corresponds to 5.2dB loss (full squares in Fig. 10(a)). This large coupling loss becomes even larger if we couple the distorted mode field into the step-index fiber (open circles in Fig. 10(a)) where the loss is more than 7.2 dB at 1050 nm.

#111521 - $15.00 USD Received 19 May 2009; revised 20 Jun 2009; accepted 22 Jun 2009; published 29 Jun 2009

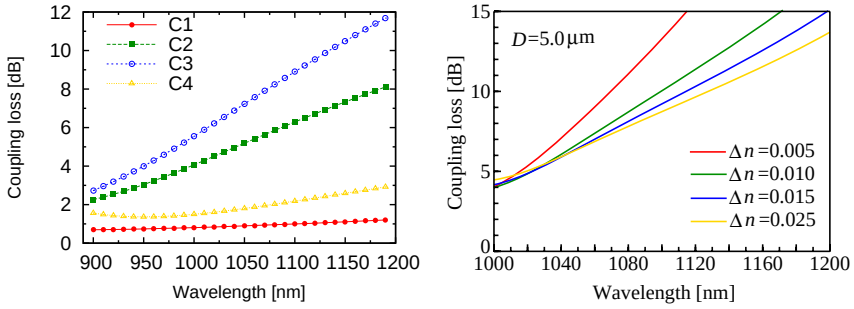

Fig. 10. (a) Coupling loss calculated from the overlap integral between LP_{01} modes of different fibers. "C1" refers to the coupling between the Bragg fiber without GTI and a step-index fiber; "C2" is the coupling between two Bragg fibers with and without GTI and both R_c is 6 μm; "C3" is the coupling between step-index and Bragg fiber with GTI and "C4" is the improved coupling between two Bragg fibers with and without GTI by changing the core size of the Bragg fiber without GTI. (b) Coupling loss as a function of wavelength between HC RDS and step index fibers with different index profiles using a core size of 5 μm.

Fortunately, this large loss can be optimized. If we take a look at the effective indices of Bragg fibers with and without GTI we can see that the difference can be considered significant and should be moved closer in order to obtain a better coupling efficiency. The effective refractive indices are 1.447329 and 1.448562 at 1040 nm for a Bragg fiber with and without GTI, respectively. If we start to decrease the core size of the regular Bragg fiber without GTI, we can decrease the effective index as well, since the wave vector of the propagating mode will enclose a smaller incident angle (see Eq. (8)). For a 4.1 μm core radius of the normal Bragg fiber the effective index is 1.447351 for LP_{01} at 1040 nm and this way the coupling loss becomes less than 1.7dB with the distorted mode (open triangles in Fig. 10(a)).

In the case of HC PBG fiber attaching simply the modified and unmodified structures will result in 4-7 dB loss along the RDS region. Using step-index fibers the loss between the HC RDS and these fibers are even larger. Fig. 10(b) shows the coupling loss between the step-index fiber with different index profiles and the HC RDS fiber where the expansion factor is set to $E = 18.7\%$. The calculations presented in Fig. 10(b) was performed with a step-index fiber having a core size of 5 μm. The coupling loss is found to be between 4 and 9 dB over the RDS range.

We can see also in Fig. 10(b) that the coupling loss can be decreased by increasing the index difference of step-index fiber. Larger mode field diameter (MFD) is presented for longer wavelengths in index guiding fibers but this larger MFD can be decreased using a fiber with larger index difference. This larger Δn however gains the possibility of multimode operation.

The calculated fiber structures are multi-moded which indicate that coupling may occur to higher order modes of the RDS fiber and may degrade the beam quality of the output if it is used for a pulse compressor. To avoid the detrimental effects due to higher order mode contents such solutions like mode conversion [22] or mode matched splice [23] are conceivable.

6. Propagation loss

The propagation loss in optical fibers can be evaluated as a sum of different type of losses such as confinement loss and scattering loss. In the case of using the fiber in a wavelength

#111521 - $15.00 USD Received 19 May 2009; revised 20 Jun 2009; accepted 22 Jun 2009; published 29 Jun 2009

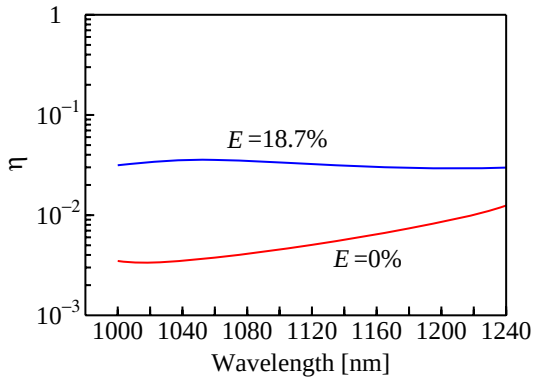

Fig. 11. The η-factor of the fundamental air-core mode as a function of wavelength with $d/\Lambda = 0.98$, $dc/\Lambda = 0.70$, $d_p/\Lambda = 0.30$, $\Lambda = 2.85$ μm, $T = t/(\Lambda - d) = 0.30$, and the expansion coefficient is set to E=0% and 18.7%.

range where the bandgap is surface-mode and leaking-mode free the dominant loss will be the scattering loss [24].

Figure 11 shows the η-factor [24, 25] of the fundamental air-core mode in HC fiber as a function of wavelength with $d/\Lambda = 0.98$, $d_c/\Lambda = 0.70$, $d_p/\Lambda = 0.30$, $\Lambda = 2.85$ μm, $t = 0.3(\Lambda - d)$, and the expansion coefficient is set to E=0% and 18.7% (see parameters in Fig. 6(c)), where the η-factor is defined as the normalized overlap integration of the power in the silica-ring as follows:

$$\eta = \frac{\int_{\text{glass annulus}} (\mathbf{E} \times \mathbf{H}^*) \cdot \hat{\mathbf{z}} dA}{\int_{\text{cross-section}} (\mathbf{E} \times \mathbf{H}^*) \cdot \hat{\mathbf{z}} dA} \tag{11}$$

The η-factor, which is proportional to the scattering loss of HC PBG fibers due to the surface roughness of the silica-ring around the air-core. In the HC PBG fiber with GTI, it is about one order of magnitude larger than the scattering loss in the HC PBG fiber without GTI.

7. Fiber nonlinearity

The fiber nonlinearity of HC PBG fibers can be almost one thousand times smaller than that of single mode fibers ($\gamma \approx 10^{-6}$ (Wm)$^{-1}$). This value was reported theoretically [8] as well as experimentally [26]. The utilization of resonant structures however may increase this value due to the increased guided mode overlap with silica.

In Fig. 12(a), we show the nonlinear coefficient γ as a function of wavelength which is a crucial quantity in high power light delivery. We use the following definition of the nonlinear coefficient [27]

$$\gamma = \gamma_{\text{air}} + \gamma_{\text{silica}} = \frac{2\pi n_{2_{\text{air}}}}{\lambda A_{\text{eff}_{\text{air}}}} + \frac{2\pi n_{2_{\text{silica}}}}{\lambda A_{\text{eff}_{\text{silica}}}} \tag{12}$$

where n_2 is the nonlinear refractive index coefficient and A_{eff} is the effective mode area calculated for air and silica, respectively, defined as [28]

$$A_{\text{eff}_i} = \frac{\left(\int_{\text{cross-section}} (\mathbf{E} \times \mathbf{H}^*) \cdot \hat{\mathbf{z}} dA\right)^2}{n_i^2 \varepsilon_0^2 c^2 \int_{A_i} |\mathbf{E}|^4 dA} \tag{13}$$

where $i =$ air or silica, ε_0 is the permittivity and c is the speed of the light in vacuum. It can be seen clearly from the results in Fig. 12 that γ is increased for the PBG fiber with GTI with an order of magnitude. The increased nonlinearity may still ensure the validity of using these

#111521 - $15.00 USD Received 19 May 2009; revised 20 Jun 2009; accepted 22 Jun 2009; published 29 Jun 2009

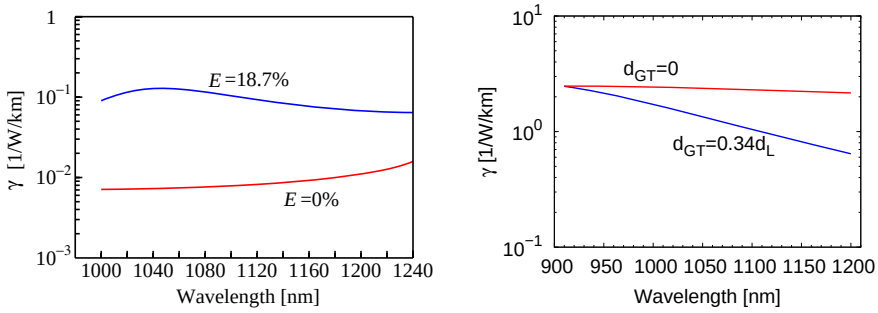

Fig. 12. The nonlinear coefficient γ as a function of wavelength in (a) a 7-cell hollow-core PBG fiber with and without core expansion and (b) in a Bragg fiber with and without resonant GTI.

fibers for high power pulse compression but the available power level with fibers using this type of resonant structure is clearly lower than using low nonlinearity HC fibers. The improvement of nonlinearity is essential in these fibers to introduce them in high intensity pulse compression though we present some solutions which still allow the generation of ultra-short and high energy pulses (Sec. 8).

In the case of SC Bragg fiber we have to account for only the second term of Eq. (12) since we can assume that the nonlinear refractive index of the different glasses are nearly the same. From the calculated $A_{\text{eff}}(\lambda)$, the plotted nonlinear coefficient shows an opposite behavior than in HC fiber (Fig. 12(b)). The nonlinearity becomes smaller in the fiber holding the resonant structure due to the larger penetration of the propagating mode into the cladding region increasing the effective area. This phenomenon is the same in the two types of fibers but the larger fraction of pulse power in the cladding at HC fibers causes the increment of pulse power in the silica having significantly larger nonlinearity than air.

We can see also that the nonlinear coefficient of HC RDS fiber is still more than a magnitude smaller than in the presented SC PBG fiber at around 1050 nm.

8. Propagation analysis

We investigate a pulse compressor consisting of two serially connected HC fibers with and without RDS. In the case of linear propagation, the necessary fiber lengths for compensating the chirp up to the third order on a broadband pulse can be estimated from the following equation-system

$$\beta_2^{(1)}L^{(1)} + \beta_2^{(2)}L^{(2)} + GDD_0 = 0 \tag{14}$$

$$\beta_3^{(1)}L^{(1)} + \beta_3^{(2)}L^{(2)} + TOD_0 = 0 \tag{15}$$

where $\beta_i^{(j)}$ is the ith order term in the Taylor series of the dispersion of the jth fiber, $L^{(j)}$ is the length of the jth fiber and GDD_0 and TOD_0 are the pulse initial GDD and third-order dispersion (TOD), respectively. It can be seen from Eq. (14) and (15) if the input chirps of the pulses are zero the pulse shape will be preserved when the ratio of the third and second order dispersion terms are same for the two fibers.

Self-phase modulation adds some additional chirps on the pulse in the case of nonlinear propagation which depends on the actual pulse power. The propagation is treated by the generalized

#111521 - $15.00 USD Received 19 May 2009; revised 20 Jun 2009; accepted 22 Jun 2009; published 29 Jun 2009

Table 1. Simulation parameters.

Parameter name	Symbol	Magnitude		Unit
Pulse parameters				
Center wavelength	λ_s	1060		nm
Spectral width	$\Delta\lambda$	16.54		nm
Energy	E_p	5-300		nJ
Input linear chirp (GDD)	GDD_0	$5\cdot10^4$, $5\cdot10^5$		fs^2
Fiber parameters				
		HC fiber	*HC RDS fiber*	
Length	L	~ 6	~ 0.7	m
Loss ($@\lambda_s$)	α	0.001	0.01	dB/m
Group delay dispersion	β_2	-0.077479	-0.058468	ps^2/m
3rd order dispersion	β_3	0.000364	-0.003086	ps^3/m
4th order dispersion	β_4	$9.8112\cdot10^{-6}$	$-4.6589\cdot10^{-5}$	ps^4/m
5th order dispersion	β_5	$2.9506\cdot10^{-7}$	$6.8492\cdot10^{-7}$	ps^5/m
Nonlinear coefficient	γ	$7\cdot10^{-6}$	10^{-4}	1/(Wm)
First moment of Raman response	T_R	1.46		fs

nonlinear Schrödinger (GNLS) equation [29]

$$\frac{\partial E(z,t)}{\partial z}+\left(\sum_{k=2}^{N}\beta_k\frac{i^{k-1}}{k!}\frac{\partial^k}{\partial t^k}\right)E+\frac{\alpha}{2}E=i\gamma\left(|E|^2E+\frac{i}{\omega_0}\frac{\partial}{\partial t}\left(|E|^2E\right)-T_RE\frac{\partial|E|^2}{\partial t}\right) \quad (16)$$

where E is the complex envelope function, z is the coordinate in the propagation direction, t is the retarded time, α is the attenuation coefficient, β_k is the kth order dispersion from the Taylor-series of the propagation constant, γ is the nonlinear coefficient and T_R is the first moment of the nonlinear Raman response. Eq. (16) is solved by the split-step Fourier method [29] such a way that the maximal phase change of the propagating pulse remained below 0.01 radian.

The used simulation parameters are listed in Table 1.

The first guess for the lengths of the fibers is taken from Eq. (14) and (15) and a brute-force optimization is used to find the highest peak power around the initial guess which target yields the possible shortest pulses with the possible highest quality [30].

We investigated the impact of the optimized compressor on incoming Gaussian pulses with $5\cdot10^4$ fs^2 input chirp and different input average powers. The transform limited input pulse width without any chirp was 100 fs ($\sim$ 16 nm bandwidth) and the temporal width became 1.4 ps adding the above chirp value. We also calculated the propagation and compression with $5\cdot10^5$ fs^2 linear input chirp resulted in 11.1 ps input full-width at half maximum (FWHM).

The dispersion parameters up to the fifth order is taken into consideration for both type of HC fibers (see Table 1). Dispersion properties of HC RDS is fitted to the dispersion function obtained from the calculations which belong to the parameters $E = 0.187$ and $T = 0.3$ (see Fig. 7). The dispersion function of the regular HC PBG fiber is fitted to a HC-1060 type fiber (see, for instance, in Ref. [20]). The β_3 parameter has a different sign in the two fibers and an approximately ten times larger absolute value for HC RDS fiber than HC-1060. The coupling loss between the two fibers is assumed to be 5 dB.

We changed the pulse energy from 5 to 175 nJ that way that the regular HC PCF was followed by the RDS fiber. This arrangement results in a pure compression quality (see Fig. 13) still at relatively low powers because the nearly transform limited shape and the high peak powers

#111521 - $15.00 USD Received 19 May 2009; revised 20 Jun 2009; accepted 22 Jun 2009; published 29 Jun 2009

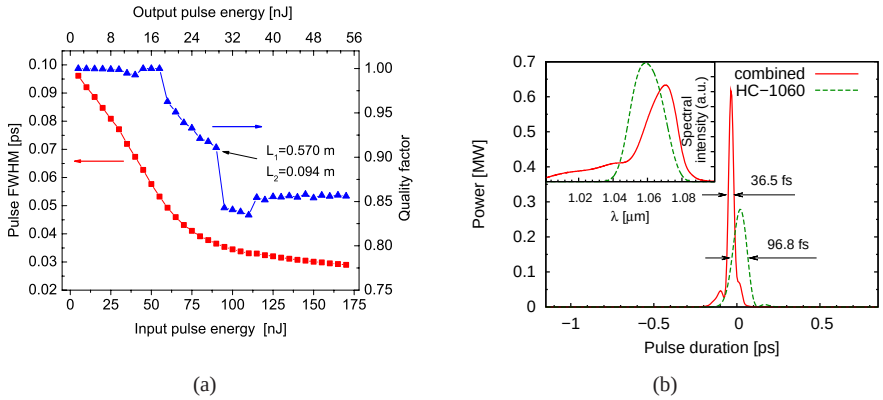

(a) (b)

Fig. 13. (a) obtained shortest pulse duration and the corresponding quality factor calculated at different input pulse energies. Optimum lengths of HC PCF (L_1) and HC RDS fiber (L_2) are shown at the point where the light energy in the main peak is 91%. (b) pulse temporal and spectral (inset) shape at the energy level (28.8 nJ). Optimum pulse shape using only non-RDS fiber shows a regular shape with only small distortions and 98.4% QF. The length of the used HC-1060 fiber was 0.63 m.

are drawn up in the RDS fiber where the nonlinearity is more than a magnitude larger than in the other HC fiber (see Sec. 7). This way a significant nonlinearity is presented at low pulse energies, too hence the output pulse FWHM is below the original transform limit. By increasing the pulse energy, the compressed pulse width rapidly decreases and QF also shows lower values. At 150 nJ input pulse energy (48 nJ output pulse energy) the pulses reach the 30 fs pulse duration due to the large self-phase modulation which broadens the spectral FWHM to 25.5 nm. The main peak of the pulse holds the 85.4% of the total pulse energy here. We depicted the obtained pulse and spectral shapes in Fig. 13(b), where the pulse energy in the main peak is just over the 90% (QF=0.91). This occurs at 28.8 nJ, which output energy corresponds to an average pulse power of 1.15 W if the pulses follow each other at a 40 MHz repetition rate. We also plotted the optimum pulse shape using only HC-1060 type fiber. It can be seen that this system does not really benefit from the utilization of HC RDS fiber although the pulse duration is shorter than the FWHM of the compressed pulse without RDS fiber. Using only HC-1060, the pulse width is also below the original transform limit and the light energy stored in the main peak is more than 98% of the total pulse energy.

It is expedient to use the RDS fiber at the first place in a serial compressor because of it's elevated nonlinearity compared to the regular HC PCF. In this arrangement the strongly chirped pulse will propagate with lower peak power through the RDS fiber avoiding large nonlinear distortions. We repeated the above calculations with the changed fiber position. The obtained result is plotted in Fig. 14(a) and 14(b). In this case the connected fibers and the regular HC fiber have nearly the same performance at 224 nJ output pulse energies.

One order of magnitude larger input chirp ($GDD_0 = 0.5$ ps^2) which is a realistic value for pulses coming out from an oscillator or amplifier is also calculated optimizing the required longer fiber lengths. These calculations are shown in Fig. 14(c) and 14(d). In this case the combined fiber compressor yields 1.5 times shorter pulses with significantly better pulse quality (QF=90.6%) compared to the performance of regular HC fibers. The HC-1060 type fiber can compress the 100 nJ pulses with 74.3% QF after 6.3 m length of propagation.

#111521 - $15.00 USD Received 19 May 2009; revised 20 Jun 2009; accepted 22 Jun 2009; published 29 Jun 2009

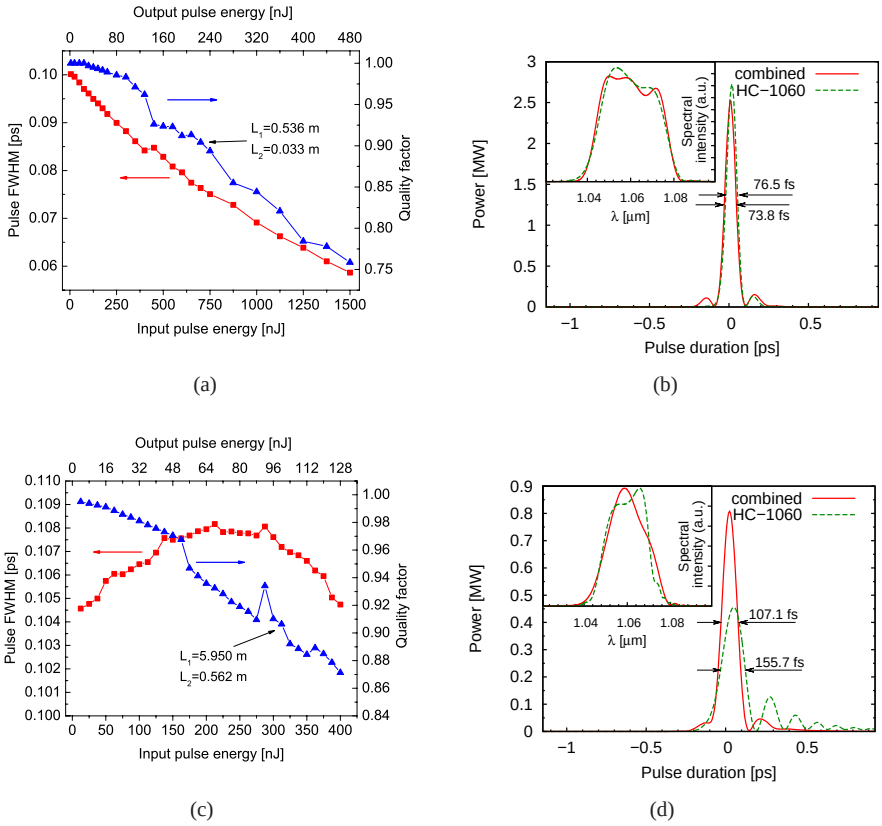

Fig. 14. (a) Pulse FWHM and quality as a function of pulse energy, (b) temporal and spectral shape at QF=90.4%, (c) pulse FWHM evaluation as a function of pulse energy with $GDD_0 = 5 \cdot 10^5$ fs^2 input chirp, (d) pulse shapes with combined and HC-1060 type fiber compressors.

9. Conclusion

We presented the theory of adopting 1D Gires-Tournois interferometers in 2D PBG structures. We demonstrated by finite element simulation that the dispersion profile of PBG fibers can be tailored effectively by the applications of resonant layers for the propagating fundamental mode. Negative dispersion slope compared to the canonical form of bandgap guidance as well as flat and nearly zero dispersion profiles can be achieved with relatively low losses. After structural optimization, low coupling losses between two fibers, with and without GTI, also can be obtained. We demonstrated that tailoring the dispersion of PBG fibers can be achieved for solid-core PBG fibers with small index difference as well as for hollow-core all-silica PBG fibers with large index difference between glass and air. The obtained dispersion profiles over 100 nm negative dispersion slope regions may yield new perspectives in dispersion management even if the increased nonlinearity and propagation loss of HC RDS fibers decrease the transmittable intensities. These properties of such fibers containing resonant structures must be further optimized to lower the nonlinearity and improve the compressed pulse quality. The propagation and the compression procedure were investigated numerically on pre-chirped, broadband Gaussian pulses showing the validity of further developments on RDS photonic bandgap fibers.

#111521 - $15.00 USD Received 19 May 2009; revised 20 Jun 2009; accepted 22 Jun 2009; published 29 Jun 2009